A Five-Switch Bridge Based Reconfigurable LLC Converter for Deeply-Depleted PEV Charging Applications

Cheng Li, *Student Member, IEEE*, Haoyu Wang, *Member, IEEE*, and Ming Shang

***Abstract*—This letter presents a reconfigurable dual LLC converter based on a five-switch bridge to charge the deeply depleted PEV onboard battery packs. Due to the reconfiguration of the primary-side switch network, two resonant tanks could operate in integrated half-bridge, half-bridge, hybrid bridge, and full-bridge modes. Thus, four operation modes are derived, with their normalized voltage gains scaled to 1:2:3:4, respectively. Those four modes enable a squeezed switching frequency span, which is close to the resonant frequency. Therefore, the efficiency performance over an ultra-wide output voltage range can be optimized. Zero-voltage-switching can be realized in all power MOSFETs over the entire load range. The operating principles, voltage gains analysis are briefed. A 1.1 kW-rated prototype converting 390V input to 100V-420V output, is designed and tested to validate the proof of concept. 97.64% peak efficiency and good efficiency over the full charging range is reported.**

***Index Terms*—circuit reconfiguration, five-switch bridge, LLC, PEV charging**

I. Introduction

The Li-ion battery is widely used in plug-in electric vehicles (PEVs) as the main energy storage unit. The typical charging profile of a deeply depleted Li-ion battery cell is plotted in Fig. 1 [1]. As indicated, the cell voltage exhibits a wide voltage range (1V-4.2V) during the whole charging process. In high-power PEV battery packs, the cell voltage range is mapped to an ultra-wide pack voltage range (typically 100V to 420V). This brings challenges to the optimal design of the dc/dc stage of the PEV onboard charger.

Frequency modulated LLC resonant converter is considered as a suitable candidate, mainly due to its attractive features such as soft switching, galvanic isolation, low EMI, and low components count [2]. However, to achieve such a wide voltage range, an ultra-wide switching frequency (f_s) range is required. This might lead to efficiency reduction, soft-switching loss, and degraded voltage regulation[3].

To narrow down the f_s range, many control schemes have been studied[4]–[6]. A variable-frequency plus phase-shift control is proposed in [4]. With phase-shift control at resonant frequency (f_r), the frequency range (f_s>f_r) is avoided and a low step-down voltage gain is achieved. In [5], a two-stage onboard charger with variable dc-link voltage is introduced. The voltage modulation range is extended, and f_s range is squeezed. However, the dc-link voltage range is limited by the front-end ac/dc stage.

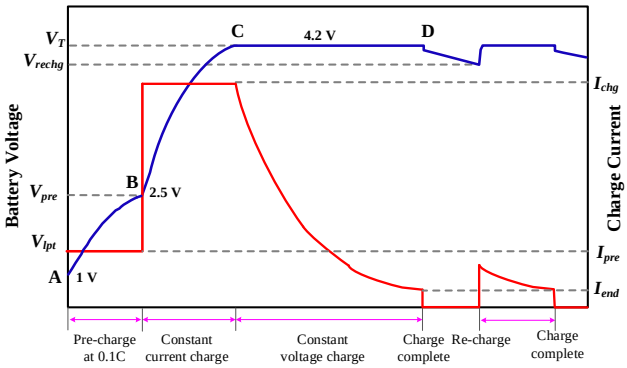

Fig. 1. Charging profile of a deeply depleted Li-ion battery cell.

Voltage modulation on the secondary side can also extend the output range with a narrow frequency span. In [7], a semi-active variable-structure rectifier is proposed. The rectifier could operate in voltage-doubler and voltage-quadrupler modes. Thus, f_s range is narrowed down. Similarly, a secondary structure with reconfigurable type-4/5/6 voltage multiplier rectifier is proposed in [8]. A squeezed frequency span is achieved with modes switch.

Another feasible solution is to switch the operation on the primary side based on the output voltage range [9], [10]. In [9], an LLC resonant converter with two resonant tanks is proposed. Two resonant tanks' secondary sides are in series. On the primary side, two resonant tanks are in series in low voltage gain mode and in parallel in high voltage gain mode. Thus, the f_s range is squeezed. In [10], a modified LLC converter with adjustable turns ratio transformer is proposed. The turns ratio could be adjusted by a bidirectional switch. Thus, four operation modes with different voltage ranges can be realized. However, the device utilization rate is relatively low.

In this letter, a reconfigurable LLC converter based on a five-switch bridge on the primary side is proposed for deeply depleted PEV battery charging applications. Its advantages include: 1) ultra-wide voltage range, 2) squeezed f_s range close to f_r, 3) full zero-voltage-switching (ZVS) over wide load range, 4) reduced conduction loss with halved resonant current (i_r), and 5) simple structure and easy to extend.

II. Proposed Converter and Operating Principles

Fig. 2 shows the schematic of the proposed LLC converter. The primary side is a reconfigurable bridge consists of five MOSFETs. Two LLC resonant tanks (RT1 and RT2) are

Manuscript received Sep 18, 2018; accepted Oct 03, 2018. This work was supported in part by the National Natural Science Foundation of China under Grant 51607113, and in part by the Shanghai Sailing Program under Grant 16YF1407600. (*Corresponding Author: Haoyu Wang.*)

C. Li is with the School of Information Science & Technology, ShanghaiTech University, Shanghai 201210, China, and also with the Chinese Academy of Sciences, Shanghai Institute of Microsystem and Information Technology, University of Chinese Academy of Sciences, Shanghai 200050, China. (e-mail: icekamp@hotmail.com)

H. Wang and M. Shang are with the Power Electronics and Renewable Energies Laboratory, ShanghaiTech University, Shanghai 201210, China (e-mail:wanghy.shanghaitech@gmail.com; shangming@shanghaitech.edu.cn).

Color versions of one or more of the figures in this paper are available online at http://ieeexplore.ieee.org.

This article has been accepted for publication in a future issue of this journal, but has not been fully edited. Content may change prior to final publication. Citation information: DOI 10.1109/TPEL.2018.2875058, IEEE Transactions on Power Electronics

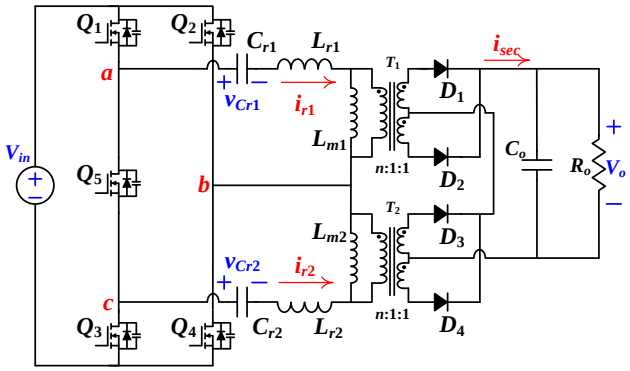

Fig. 2. Schematic of the proposed converter.

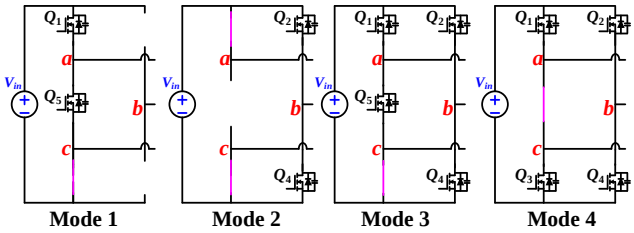

Fig. 3. Operation modes of the five-switch bridge.

connected with this five-switch bridge. It should be noted that the parameters including resonant inductances (L_r), resonant capacitances (C_r), magnetizing inductances (L_m), and transformer turns ratio (n) in those two resonant tanks are identical. On the secondary side, two center-tapped full wave rectifiers are in series. By configuring the primary-side MOSFETs in ON or OFF states, the inputs of the resonant tanks can be configured as full-bridge or half-bridge. Therefore, four combinations of switch patterns lead to four operation modes. The primary-side circuits of those four operation modes are plotted in Fig. 3.

Mode 1: In Mode 1, Q_3 is constantly ON while $Q_{2,4}$ are constantly OFF; Q_1 and Q_3 are driven complementarily with certain deadband. RT1 and RT2 are in series and integrated into one resonant tank. This integrated resonant tank operates in half-bridge mode and its input (v_{ac}) is a two-level (0 to V_{in}) square wave. v_{ac}'s root-mean-square (RMS) value is $V_{in}/2$.

Mode 2: In Mode 2, $Q_{1,3}$ are constantly ON while Q_5 is constantly OFF; Q_2 and Q_4 are driven complementarily with certain deadband. Therefore, the inputs of RT1 and RT2 (v_{ab} and v_{cb}) are both two-level square waves: 0 to V_{in}, and -V_{in} to 0, respectively. This means both resonant tanks operate in half-bridge mode. v_{ab} and v_{cb}'s RMS values are both $V_{in}/2$.

Mode 3: In Mode 3, Q_3 is constantly ON; $Q_{1,4}$ and $Q_{2,5}$ are driven complementarily with certain deadband. Therefore, v_{ab} and v_{cb} are both two-level square waves: -V_{in} to V_{in}, and -V_{in} to 0, respectively. This means RT1 operates in full-bridge mode while RT2 operates in half-bridge mode. v_{ab} and v_{cb}'s RMS values are V_{in} and $V_{in}/2$, respectively. The power sharing between two resonant tanks are mismatched. Hence, equivalent load resistance (R_e) and equivalent output voltage in two resonant tanks are also mismatched.

Mode 4: In Mode 4, Q_5 is constantly ON; $Q_{1,4}$ and $Q_{2,3}$ are driven complementarily with certain deadband. Therefore, the input of RT1 and RT2 (v_{ab} and v_{cb}) is a two-level (-V_{in} to V_{in}) square wave. Both resonant tanks operate in full-bridge mode. v_{ab} and v_{cb}'s RMS values are both V_{in}.

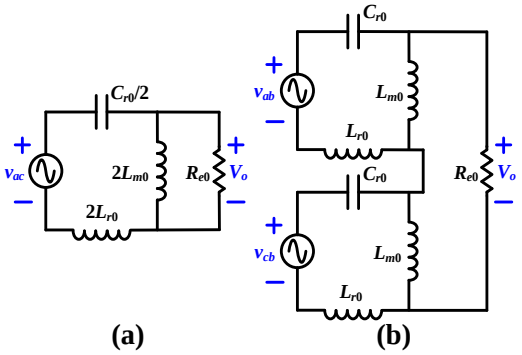

Fig. 4. Equivalent circuit model: (a) mode 1, and (b) modes 2-4.

Table I
RESONANT PARAMETERS AND VOLTAGE GAIN

Mode	**1**	**2**		**3**		**4**	
Resonant tanks	1	2		2		2	
Q	Q_0	Q_0	Q_0	$1.5Q_0$	$0.75Q_0$	Q_0	Q_0
m	m_0	m_0	m_0	m_0	m_0	m_0	m_0
$v_{g,rms}$	$V_{in}/2$	$V_{in}/2$	$V_{in}/2$	$V_{in}/2$	V_{in}	V_{in}	V_{in}
Gain	G_0	$2G_0$		$3G_0$		$4G_0$	

III. VOLTAGE GAIN ANALYSIS

Using the first harmonic approximation (FHA) method, the equivalent sinusoidal circuit models of the proposed circuit in four modes are derived as shown in Fig. 4. R_{e0} is expressed.

$$R_{e0} = \frac{8n^2}{\pi^2} R_o \tag{1}$$

The key parameters of the resonant tanks in four modes are summarized in Table I. In Table I, $v_{g,rms}$ is the RMS value of the resonant tank's input voltage; Q is the quality factor; m is the inductance ratio.

As indicated in Fig. 4 (a), two resonant tanks are in series and construct an integrated resonance tank in Mode 1. The equivalent L_m and L_r are both doubled, the equivalent C_r is halved, and R_e is R_{e0}. Thus,

$$Q_1 = \frac{\sqrt{2L_{r0}/(C_{r0}/2)}}{R_{e0}} = 2\frac{\sqrt{L_{r0}/C_{r0}}}{R_{e0}} = Q_0 \tag{2}$$

$$m_1 = 2L_{m0}/(2L_{r0}) = L_{m0}/L_{r0} = m_0 \tag{3}$$

In Modes 2 and 4 [Fig. 4 (b)], both resonant tanks deliver equal power to the load. Thus, R_e for both resonant tanks is $R_{e0}/2$. Q and m in two resonant tanks are matched.

$$Q_2 = Q_4 = \frac{\sqrt{L_r/C_r}}{R_e/2} = Q_0 \tag{4}$$

$$m_2 = m_4 = L_{m0}/L_{r0} = m_0 \tag{5}$$

In Mode 3, the power sharing between two resonant tanks are mismatched. R_e of RT1 and RT2 are derived as $2R_{e0}/3$ and $R_{e0}/3$, respectively. It should be noted that Q is also mismatched while m is still matched.

This article has been accepted for publication in a future issue of this journal, but has not been fully edited. Content may change prior to final publication. Citation information: DOI 10.1109/TPEL.2018.2875058, IEEE Transactions on Power Electronics

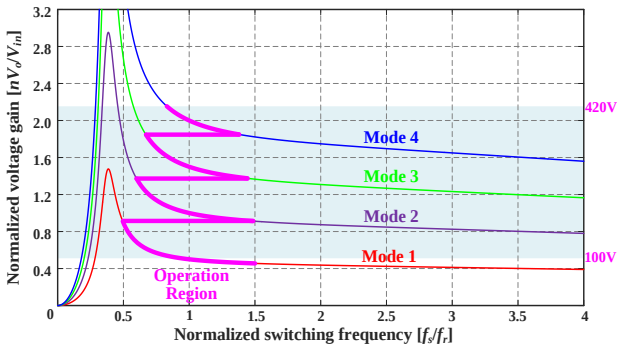

Fig. 5. Voltage gain curves versus normalized f_s.

$$Q_{3\_1} = \frac{\sqrt{L_r / C_r}}{2R_e / 3} = 0.75Q_0 \tag{6}$$

$$Q_{3\_2} = \frac{\sqrt{L_r / C_r}}{R_e / 3} = 1.5Q_0 \tag{7}$$

$$m_{3\_1} = m_{3\_2} = L_{m0} / L_{r0} = m_0 \tag{8}$$

According to FHA method and equivalent sinusoidal circuit models, the voltage gain of resonant tank G_{LLC} is derived.

$$G_{LLC} = \frac{mf_n^2}{\sqrt{[(m+1)f_n^2 - 1]^2 + m^2Q^2 f_n^2 (f_n^2 - 1)^2}} \tag{9}$$

Where f_n is the normalized switching frequency, f_s/f_r.

As aforementioned, due to identical Q and m, G_{LLC} in modes 1, 2, and 4 are the same (G_{LLC0}). In Mode 3, Q_{3_1} is smaller than Q_0 while Q_{3_2} is larger than Q_0. Accordingly, the relationships in between G_{LLC} in four modes are expressed.

$$G_{LLC3\_1} > G_{LLC1} = G_{LLC2} = G_{LLC4} = G_{LLC0} > G_{LLC3\_2} \tag{10}$$

However, the total G_{LLC} in Mode 3, (G_{LLC3_1}+G_{LLC3_1}), is approximately $2G_{LLC0}$. Hence, G_{LLC} in four modes is considered to be identical. The overall voltage gain is determined by $v_{g,rms}$ and the number of resonant tanks. In Mode 1, the voltage gain of the proposed converter is defined as G_0. Thus, the voltage gains in mode 2, 3, and 4 are derived as $2G_0$, $3G_0$, and $4G_0$, respectively.

Correspondingly, the curves of normalized voltage gain versus normalized f_s in four modes are plotted in Fig. 5. As indicated, the mode transition facilitates both squeezed f_s range and extended voltage gain range. Thus, the efficiency performance over the wide output voltage range can be enhanced and the design complexity can be reduced.

IV. Experiment Verification

A 1.1 kW scale-down laboratory prototype for PEV deeply depleted charging is built to verify the effectiveness of the proposed converter. V_{in} = 390 V, V_o = 100–420 V. Q_1–Q_5: SCT3120, D_1–D_4: C3D10060A, transformers' turns ratio n = 2:1, L_{m1} = L_{m2} = 382 μH, L_{r1} = L_{r2} = 62 μH, C_{r1} = C_{r2} = 32 nF, f_r = 100 kHz, and f_s range is 50-150 kHz. At pre-charging stage, the charging current (I_o) is 1.05A. At regular constant current (CC) charging stage, I_o is 2.62A.

The steady-state waveforms in Mode 1 is captured in Fig. 6. As shown, v_{ac} is a two-level (0V to 390V) square wave in half-bridge mode. i_{r1} equals $-i_{r2}$, which agrees well with the previous

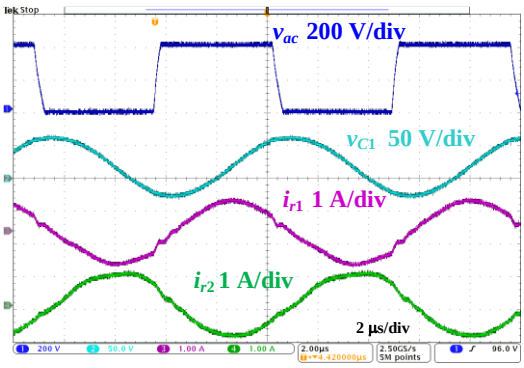

Fig. 6. Steady-state waveforms in Mode 1, V_o=100V, P_o=105W.

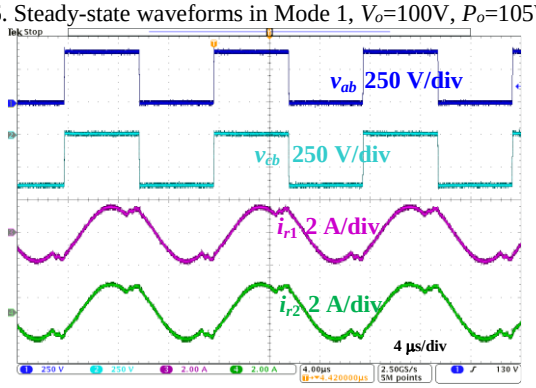

Fig. 7. Steady-state waveforms in Mode 2, V_o=230V, P_o=242W.

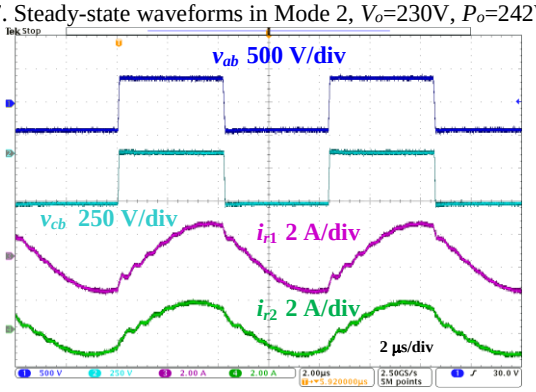

Fig. 8. Steady-state waveforms in Mode 3, V_o=300V, P_o=786W.

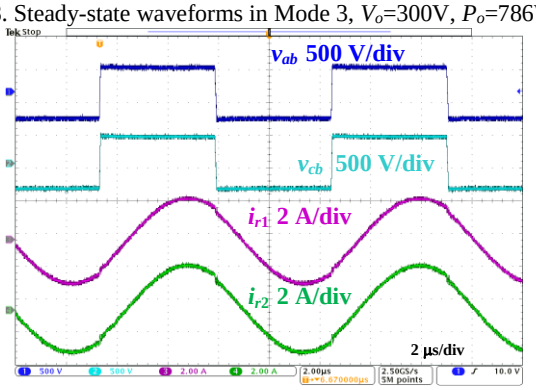

Fig. 9. Steady-state waveforms in Mode 4, V_o=417V, P_o=1.1kW.

mode analysis. The steady-state waveforms in Mode 2 is captured in Fig. 7. As shown, v_{ab} and v_{cb} are both two-level square waves (0V to 390V and -390V to 0V) in half-bridge mode. i_{r1} equals i_{r2}. This means that the power sharing between two resonant tanks are matched.

The steady-state waveforms in Mode 3 is captured in Fig. 8. As shown, v_{ab} is a two-level (-390V to 390V) square wave, while v_{cb} is a two-level (-390V to 0V) square wave. i_{r1} is larger

This article has been accepted for publication in a future issue of this journal, but has not been fully edited. Content may change prior to final publication. Citation information: DOI 10.1109/TPEL.2018.2875058, IEEE Transactions on Power Electronics

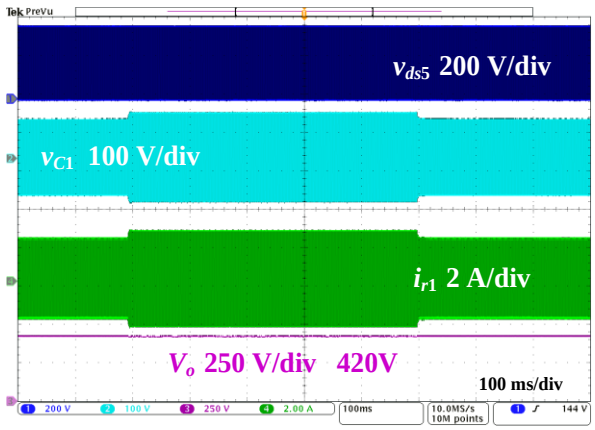

Fig. 10. Waveforms of voltage dynamic response in CV stage.

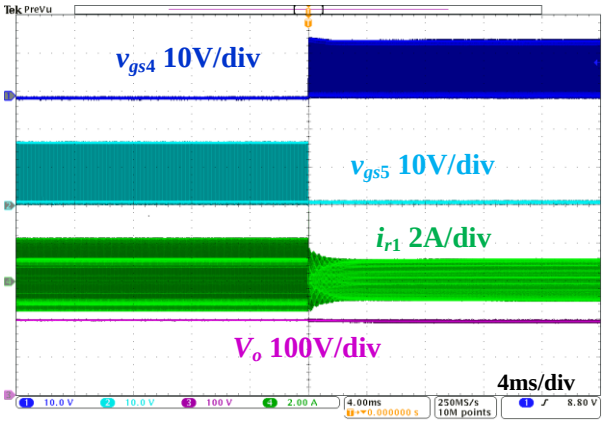

Fig. 11. Waveforms of mode transition from Mode 1 to Mode 2.

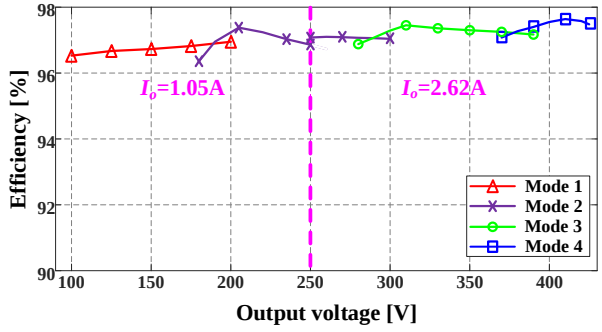

Fig. 12. Efficiency versus V_o in pre-charge and CC stage.

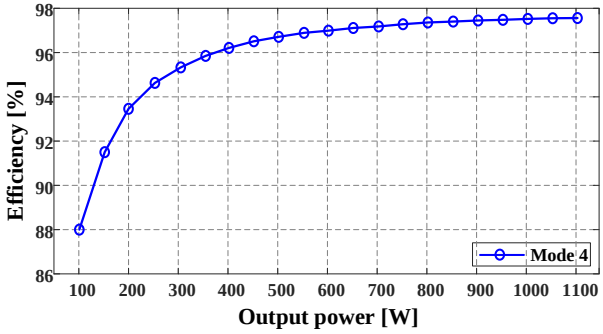

Fig. 13. Efficiency versus P_o in CV stage, V_o = 420 V.

than i_{r2}. This means RT1 delivers higher power than RT2. The main reason is that RT1 operates in full-bridge mode while RT2 operates in half-bridge mode. The steady-state waveforms in Mode 4 is captured in Fig. 9. As shown, v_{ab} and v_{cb} are both two-level (-390V to 390V) square waves in full-bridge mode. i_{r1} equals i_{r2}. This indicates that the power sharing between two resonant tanks are matched.

Fig. 10 demonstrates the dynamic response in constant voltage (CV) charging stage. The converter operates in Mode 4. V_o is well regulated to 420 V when load variation occurs. Fig. 11 demonstrates a smooth transition from Mode 1 to Mode 2 in CC charging stage. In summary, both CC and CV operations demonstrate a robust dynamic response.

Fig. 12 provides the measured efficiency data in pre-charge and CC charging stages. As shown, when V_o increases, the operation mode changes from 1 to 4, accordingly. 190V, 290V, and 380V mark the three mode transition points. Beyond those points, the latter mode demonstrates higher efficiency than the former mode. This is because the latter mode enables an f_s span closer to f_r. Thus, the circuit operation is more optimized. 250V is the boundary between the precharge and CC charging stages where I_o steps from 1.05A to 2.62A. The converter demonstrates 97.64% peak efficiency and good overall efficiency.

Fig. 13 provides the measured efficiency data in the CV charging stage. As shown, the converter demonstrates 97.56% peak efficiency and good overall efficiency.

V. Conclusion

In this letter, a novel five-switch bridge based reconfigurable dual LLC converter is proposed for PEV deeply depleted battery charging applications. By adding only one extra MOSFET, the proposed converter could operate in four different modes with scaled voltage gain. Thus, it could provide an ultra-wide voltage range. With frequency modulation, f_s is constrained to be close to f_r over the entire output range. Thus, the efficiency performance can be enhanced over the full load range. A 1.1 kW experimental prototype with 390 V input and 100–420 V output is built to verify the concept. The proposed converter is also suitable for other wide input/output voltage range applications and is compatible with other control methods and secondary rectifiers.

References

[1] H. Wang, S. Dusmez, and A. Khaligh, "A novel approach to design EV battery chargers using SEPIC PFC stage and optimal operating point tracking technique for LLC converter," in *2014 IEEE Applied Power Electronics Conference and Exposition*, pp. 1683–1689.

[2] J. Deng, S. Li, S. Hu, C. C. Mi, and R. Ma, "Design methodology of LLC resonant converters for electric vehicle battery chargers," *IEEE Trans. Veh. Technol.*, vol. 63, no. 4, pp. 1581–1592, May 2014.

[3] X. Sun, X. Li, Y. Shen, B. Wang, and X. Guo, "Dual-Bridge LLC Resonant Converter With Fixed-Frequency PWM Control for Wide Input Applications," *IEEE Trans. Power Electron.*, vol. 32, no. 1, pp. 69–80, Jan. 2017.

[4] H. Wu, X. Zhan, and Y. Xing, "Interleaved LLC Resonant Converter With Hybrid Rectifier and Variable-Frequency Plus Phase-Shift Control for Wide Output Voltage Range Applications," *IEEE Trans. Power Electron.*, vol. 32, no. 6, pp. 4246–4257, Jun. 2017.

[5] Z. Liu, B. Li, F. C. Lee, and Q. Li, "High-Efficiency High-Density Critical Mode Rectifier/Inverter for WBG-Device-Based On-Board Charger," *IEEE Trans. Ind. Electron.*, vol. 64, no. 11, pp. 9114–9123, Nov. 2017.

[6] H. Wang, S. Dusmez, and A. Khaligh, "Maximum Efficiency Point Tracking Technique for LLC -Based PEV Chargers Through Variable DC Link Control," *IEEE Trans. Ind. Electron.*, vol. 61, no. 11, pp. 6041–6049, 2014.

[7] H. Wu, Y. Li, and Y. Xing, "LLC Resonant Converter With Semiactive Variable-Structure Rectifier (SA-VSR) for Wide Output Voltage Range Application," *IEEE Trans. Power Electron.*, vol. 31, no. 5, pp. 3389–3394, May 2016.

[8] M. Shang, H. Wang, and Q. Cao, "Reconfigurable LLC Topology With Squeezed Frequency Span for High-Voltage Bus-Based Photovoltaic Systems," *IEEE Trans. Power Electron.*, vol. 33, no. 5, pp. 3688–3692, May 2018.

[9] C.-E. Kim, J.-I. Baek, and J.-B. Lee, "High-Efficiency Single-Stage LLC Resonant Converter for Wide-Input-Voltage Range," *IEEE Trans. Power Electron.*, vol. 33, no. 9, pp. 7832–7840, Sep. 2018.

[10] H. Hu, X. Fang, F. Chen, Z. J. Shen, and I. Batarseh, "A Modified High-Efficiency LLC Converter With Two Transformers for Wide Input-Voltage Range Applications," *IEEE Trans. Power Electron.*, vol. 28, no. 4, pp. 1946–1960, Apr. 2013.